

## Diffusion in correlated random potentials, with applications to DNA

Michael Slutsky,<sup>1,\*</sup> Mehran Kardar,<sup>1</sup> and Leonid A. Mirny<sup>1,2</sup>

<sup>1</sup>*Department of Physics, Massachusetts Institute of Technology, 77 Massachusetts Avenue, Cambridge, Massachusetts 02139, USA*

<sup>2</sup>*Harvard-MIT Division of Health Sciences and Technology, Massachusetts Institute of Technology, 77 Massachusetts Avenue, Cambridge, Massachusetts 02139, USA*

(Received 10 October 2003; published 1 June 2004)

Many biological processes involve one-dimensional diffusion over a correlated inhomogeneous energy landscape with a correlation length  $\xi_c$ . Typical examples are specific protein target location on DNA, nucleosome repositioning, or DNA translocation through a nanopore, in all cases with  $\xi_c \approx 10$  nm. We investigate such transport processes by the mean first passage time (MFPT) formalism, and find diffusion times which exhibit strong sample to sample fluctuations. For a displacement  $N$ , the average MFPT is diffusive, while its standard deviation over the ensemble of energy profiles scales as  $N^{3/2}$  with a large prefactor. Fluctuations are thus dominant for displacements smaller than a characteristic  $N_c \gg \xi_c$ : typical values are much less than the mean, and governed by an anomalous diffusion rule. Potential biological consequences of such random walks, composed of rapid scans in the vicinity of favorable energy valleys and occasional jumps to further valleys, is discussed.

DOI: 10.1103/PhysRevE.69.061903

PACS number(s): 87.10.+e, 87.14.Gg, 87.15.Vv, 05.40.Fb

### I. INTRODUCTION

Diffusion appears in most basic processes in the living matter and therefore has been studied extensively by theoretical and experimental biophysicists for many decades. At the macroscopic scale, the phenomena are adequately described by continuum models that form a well established methodology finding many applications in science and technology [1]. Advanced experimental methods, such as nanoprobeing and single-molecule techniques, provide us with a wealth of data at the microscopic level. Theoretical description of the observed phenomena at such scales is often a considerable challenge, since many irregular features that average out on the macroscopic scale cannot be ignored anymore. Sometimes, however, rather simple characteristics emerge, allowing for exact analytic treatment.

One-dimensional (1D) transport is rarely found on the macroscopic scale; at the molecular level though, one can find several examples, e.g., kinesin motion along microtubules [2–4] or DNA translocation through a nanopore [5–8]. Usually, in such problems, the underlying potential profile is considered to be constant or at least regular. However, as we show in this paper, DNA sequence heterogeneity and the resulting random energy landscape can have a considerable influence on the diffusion up to biologically relevant length scales at room temperatures.

#### A. Protein-DNA interaction

The first example we study here arises in the context of protein-DNA interaction. As proposed by von Hippel and Berg [9,10], and recently observed in many systems [11], 1D “sliding” of proteins along the DNA molecule is an important component of protein specific site location; at least in

prokaryotes. The sliding is viewed as an unbiased, thermally activated process. The actual rules of motion for sliding depend on the details of interaction between the protein and the DNA. The general belief is that there are two protein-DNA binding modes: a strong “specific” mode that characterizes binding of operator sites, and a much weaker “nonspecific” mode in which binding of noncognate DNA occurs [10,12–14]. In the nonspecific or “search” mode, the interaction energy is usually assumed to be independent of the DNA sequence that the protein is bound to, though not much experimental evidence beside relatively fast observed search times favors this strictly “equipotential” picture. On the other hand, scanning force microscopy experiments by Erie *et al.* [15] clearly demonstrate DNA bending by *Cro* repressor protein, both at operator and at nonoperator sequences [39]. Since local DNA elasticity is known to be highly sequence-dependent [16], the energy of protein bound at random locations should have a random component, correlated at length scales of the order of the protein binding domain size; see Fig. 1(a). This sequence-dependent interaction energy component appears in addition to possible local uncorrelated sequence-dependent contributions from amino acid-base pair contacts.

To estimate the significance of the random component of the elastic energy, we use DNA elasticity data supplied by the BEND.IT server [17], that incorporates DNase I based bendability parameters [18] and the consensus bendability scale [19]. We assume that the protein-DNA complex in Fig. 1(a) has a fixed geometry, i.e., the protein is “hard.” Then, the elastic contribution to the protein-DNA interaction energy at the  $i$ th sequence has a random component proportional to the random component of the Young’s modulus  $\delta E_i$ :

$$U_i = \left[ 1 + \frac{\delta E_i}{\bar{E}} \right] \left( \frac{\ell_p \theta^2}{2L} \right) k_B T, \quad (1)$$

where  $\ell_p \approx 50$  nm is the DNA persistence length,  $\theta \approx 60^\circ$  is the curvature angle [15],  $L = 10$ – $20$  bp is the bent sequence

\*Electronic address: mich@mit.edu

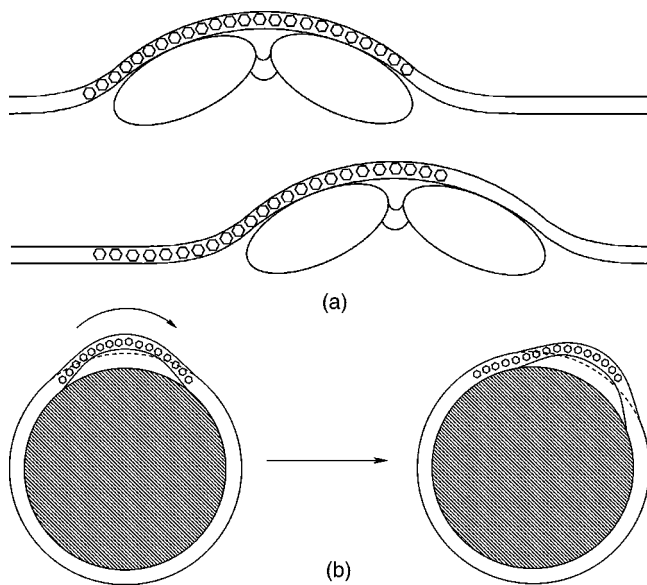


FIG. 1. (a) Prokaryotic transcription factor sliding; (b) nucleosome repositioning.

length and  $\bar{E} \approx 3.4 \times 10^8$  N/m is the average Young's modulus. The resulting potential profile is plotted in Fig. 2(a). The standard deviation of the elastic energy induced by the Young's modulus variations (10–15 % typically) for biologically relevant parameters is  $\langle (\delta U)^2 \rangle^{1/2} \sim 0.5-1.5 k_B T$ , so that disorder appears to be relevant for this problem. Fig-

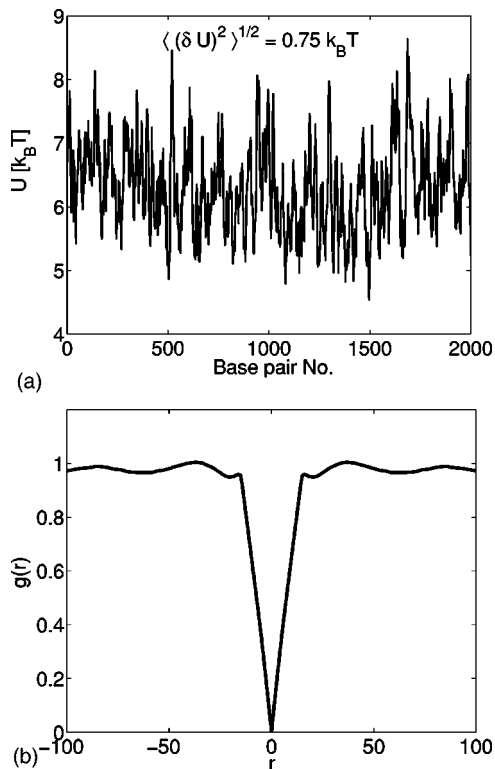


FIG. 2. (a) Energy of local elastic deformation and (b) potential profile correlator, as calculated from the data supplied by the server BEND.IT for a segment of *E.coli* genome. The deformed DNA sequence is assumed to be of length  $L=15$  bp.

ure 2(b) shows the normalized energy-energy correlator for the random energy component

$$g(r) = \frac{1}{2\langle \delta U^2(x) \rangle} \langle [\delta U(x) - \delta U(x+r)]^2 \rangle, \quad (2)$$

averaged over 10 000 DNA sequences. Saturation to  $g(r) \approx 1$  is clearly observed on the scale of 15 base pairs, which is the correlation length of this potential profile.

Another interesting example, also from the field of protein-DNA interaction, was considered recently by Schiesl *et al.* [20], and deals with nucleosome repositioning by DNA reptation. It was argued that chromatin remodeling [21,22] can be readily understood in terms of intranucleosomal loop diffusion, the size of the loop resulting mainly from a compromise between elastic energy and nucleosome-DNA binding energy. Here again, for a given size of the loop, the elastic energy is sequence dependent [22], and therefore has a random component with finite correlation length; see Fig. 1(b). For nucleosome repositioning, this effect may be even more pronounced than for prokaryotic protein-DNA interaction; the bending angles  $\theta$  and the sequence lengths  $L$  are 2 to 3 times larger so that the net effect may be twice as strong as for the *Cro* repressor [20].

It is known that DNA can have an *intrinsic* curvature arising from the stacking interactions between base pairs. Such sequence-dependent curvature can play a role similar to sequence-dependent DNA bendability in providing a correlated landscape. The bending energy of an intrinsically curved region is easier, requiring a smaller angular deformation  $\theta = \theta_{\text{complex}} - \theta_{\text{intrinsic}}$  by the DNA-protein complex. Such sequence-dependent intrinsic curvature was suggested to be involved in positioning nucleosomes [23].

Aside from DNA bendability and curvature, local correlations in nucleotide composition, known to be present in eukaryotic genomes, (AT/GC-rich isochores) can result in a correlated landscape of the protein-DNA binding energy. This effect becomes especially pronounced when a DNA-binding protein has a strong preference toward a particular AT/GC composition of its site. However, in this case, variations take place over much longer scales, and are not quantitatively relevant in the specific contexts addressed in this paper.

Both above examples can be viewed as specific cases of DNA reptation by means of a propagating defect (or “slack”) of a fixed size. Elastic energy associated with the slack creation is sequence-dependent and correlated on the scale of the slack size. The propagating defect is well localized and samples the energies of well-defined subsequent DNA segments. As was pointed out by Cule and Hwa [24], short-range correlated randomness of this kind has no effect on the scaling of the reptation time. However, as we show below, the defect motion itself is strongly influenced by the disorder and has nontrivial behavior at different length scales.

### B. DNA translocation through a nanopore

Consider a piece of single-stranded DNA (ssDNA) passing through a large membrane channel. If the potential difference across the membrane is zero, the motion of the ss-

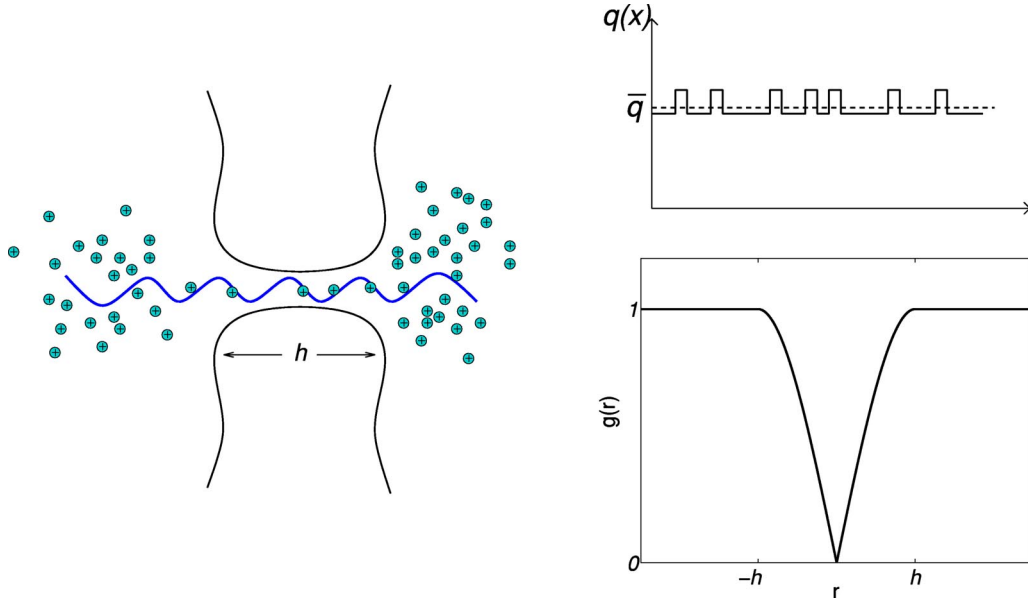


FIG. 3. (Color online) ssDNA transport through the nanopore; on the right: charge density  $q(x)$  and correlator  $g(r) = \langle [\delta U(x) - \delta U(x+r)]^2 \rangle / (2\langle \delta U^2(x) \rangle)$  as a function of the coordinate  $r$ .

DNA is governed by thermal fluctuations. Since the channel width differs from the ssDNA external diameter only by few Ångströms [40], it is reasonable that local interactions between the nucleotides and the amino acids of the channel take place. These interactions may have a local base-dependent component. In addition, longer-range terms are likely to appear in the presence of a voltage difference. In the cytoplasm, the DNA negative charge is almost completely screened out at distances of few nanometers by the counterion cloud. When the DNA molecule enters the pore, most of the counterions are likely to be “shaven off,” though some of them may remain stuck to the DNA; see Fig. 3. Thus, the linear charge density inside the pore acquires a random and basically uncorrelated component:

$$q(x) = \bar{q}(x) + \delta q(x), \quad \langle \delta q(x) \delta q(y) \rangle = \rho^2 a \delta(x - y), \quad (3)$$

where  $a = 0.34$  nm is the interbase distance. The potential energy of the DNA segment inside the pore in the presence of a voltage difference of  $V_0$  is

$$U(x) = \frac{V_0}{h} \int_0^h x' q(x + x') dx'. \quad (4)$$

Since the average charge density  $\bar{q}(x)$  is in general nonzero, DNA transport is driven by the average force  $V_0 \bar{q}(x)/h$ . The correlation function of the random component of  $U(x)$  is readily calculated to be

$$\langle \delta U(x) \delta U(x+y) \rangle = \frac{V_0^2 \rho^2 a}{3h^2} (h - |y|)^2 \left( h + \frac{|y|}{2} \right) H(h - |y|), \quad (5)$$

where  $H(x)$  is the Heaviside function. Thus, the potential profile for DNA motion has a random component with correlation length of  $h$ . Taking  $V_0 \sim 100$  mV,  $\rho \sim e/h$  ( $e$  is the

elementary charge),  $h \sim 10$  nm, we obtain  $\delta U \sim k_B T$ .

Although this example differs from the above ones in that a nonzero average driving force is present, large random fluctuations of the energy landscape may have significant effect on the distribution of translocation times — a problem that has attracted much interest lately [25].

## II. DIFFUSION IN A RANDOM POTENTIAL

### A. The model

The problems described above map onto a one-dimensional random walk with position-dependent hopping probabilities  $p_i$ ,  $q_i = 1 - p_i$  to the right and to the left, respectively; it is most natural to assume the regular activated transport form

$$p_i \propto e^{-\beta(U_{i+1} - U_i)}, \quad q_i \propto e^{-\beta(U_{i-1} - U_i)}, \quad (6)$$

where  $\beta \equiv (k_B T)^{-1}$  and  $U_i$  is the sequence-dependent component of the potential energy. The latter is basically a sum of many random contributions and can therefore be considered to be normally distributed [13]. Thus, in the absence of correlations, the probability for realization of a certain profile  $U(x)$  of length  $L$  is (in the continuum limit)

$$P[U(x)] \propto \exp \left[ -\frac{\alpha}{2} \int_0^L dx U^2(x) \right]. \quad (7)$$

This is the well-known random-energy model [26] that was applied successfully to various biophysical problems, from protein folding [27] to protein-DNA interaction [13]. It assumes no correlations between energies of different sites. One can think of a more general form of potential profile

$$P[U(x)] \propto \exp \left[ -\frac{1}{2} \int_0^L \int_0^L dy dx U(x) G(x-y) U(y) \right]. \quad (8)$$

Taking for example,  $G(x-y) \propto \delta_{xy}^2 \delta(x-y)$ , we obtain the random-force model [28] that describes an energy landscape appearing as a random walk with linearly growing correlations. This model was studied during the last decades in the context of heteropolymer dynamics [24,29], glassy systems [30,31] and quite recently—to describe DNA denaturation dynamics [32]. Characteristic features of the random-force model are logarithmically slow (“Sinai’s”) diffusion [33,34] and aging [31,32]. More generally,  $G$  is related to the correlator of  $U$  by  $\langle U(x)U(y) \rangle = G^{-1}(x-y)$ .

To include finite-range correlations into Eq. (7), we must incorporate a limitation on the acceptable forces. The ensemble of energy profiles is therefore naturally described by the following probability density:

$$P[U(x)] \propto e^{-\mathcal{H}[U]}, \quad (9a)$$

with *pseudoenergy*

$$\mathcal{H}[U] = \frac{1}{2} \int_0^L dx \left[ \alpha U^2(x) + \gamma \left( \frac{dU}{dx} \right)^2 \right]. \quad (9b)$$

Energy level statistics for this kind of potential profile is also Gaussian, as can be seen from the average

$$\langle e^{ikU} \rangle = \frac{\int \mathcal{D}[U] e^{ikU} e^{-\mathcal{H}[U]}}{\int \mathcal{D}[U] e^{-\mathcal{H}[U]}} = \exp \left( -\frac{k^2}{4\sqrt{\alpha\gamma}} \right), \quad (10)$$

which is the characteristic function for Gaussian distribution with zero mean and variance

$$\sigma^2 = \frac{1}{2\pi} \int_{-\infty}^{\infty} \frac{dq}{\alpha + \gamma q^2} = \frac{1}{2\sqrt{\alpha\gamma}}. \quad (11)$$

The correlator of the potential profile is readily calculated as

$$g(r) \equiv \frac{1}{2} \langle [U(x) - U(x+r)]^2 \rangle = \sigma^2 (1 - e^{-|r|/\xi_c}), \quad (12)$$

where  $\xi_c = \sqrt{\gamma/\alpha}$  is the correlation length.

### B. Mean first passage time

A convenient formalism for analyzing diffusion in a random one-dimensional potential profile is that of mean first-passage time [34,35]. For a given set of probabilities  $\{p_i\}$ , the MFPT from  $i=0$  to  $i=N$  (in terms of number of steps) is

$$\bar{t}_{0,N} = N + \sum_{k=0}^{N-1} \omega_k + \sum_{k=0}^{N-2} \sum_{i=k+1}^{N-1} (1 + \omega_k) \prod_{j=k+1}^i \omega_j, \quad (13)$$

where  $\omega_i \equiv q_i/p_i$  (see Appendix A for derivation). The MFPT given by this expression is for a fixed realization of probabilities, i.e., for a given potential energy profile; as such, it is itself a random variable. The disorder-averaged version of

the MFPT is readily obtained after we note that the sequential products in Eq. (13) reduce to

$$\prod_{j=k}^i \omega_j = \exp[\beta(U_{i+1} + U_i - U_k - U_{k-1})]. \quad (14)$$

For an uncorrelated potential profile, this exponential factorizes into independent exponentials; after the ensemble averaging and the summations are carried out, we obtain for  $N \gg 1$ ,

$$\langle \bar{t}_{0,N} \rangle = N^2 e^{2\beta^2 \sigma^2}, \quad (15)$$

where, for the uncorrelated potential ( $\gamma=0$ )

$$\sigma^2 = \frac{1}{\alpha a}. \quad (16)$$

Note that this expression cannot be obtained by simply putting  $\gamma=0$  in Eq. (11). The reason is that when  $\gamma$  becomes small, the discrete nature of the underlying lattice (the DNA) starts to matter. The integration in the Fourier space in Eq. (11) extends only up to  $|q_{\max}| = \pi/a$ , and thus,

$$\sigma^2|_{\gamma \rightarrow 0} = \int_{-\pi/a}^{\pi/a} \frac{dq}{2\pi\alpha} = \frac{1}{\alpha a}. \quad (17)$$

Returning to the case of a finite correlation length, we note that in the limit of  $\xi_c \gg a$ , variations of the potential between neighboring sites can be neglected compared to variations between sites separated by distances of order  $\xi_c$  or larger. Since the main contribution to the MFPT comes from the double sum in Eq. (13), we can write the continuum version as

$$\bar{t}_{0,N} \approx 2 \int_0^N dx \int_x^N dy e^{2\beta[U(x)-U(y)]}. \quad (18)$$

To average over all possible realizations of  $\{U(x)\}$ , we calculate

$$\begin{aligned} \langle e^{2\beta[U(x)-U(y)]} \rangle &= \frac{\int \mathcal{D}[U] e^{2\beta[U(y)-U(x)]} e^{-\mathcal{H}[U]}}{\int \mathcal{D}[U] e^{-\mathcal{H}[U]}} \\ &= \exp \left[ \frac{2\beta^2 \xi_c}{\gamma} (1 - e^{-|x-y|/\xi_c}) \right]. \end{aligned} \quad (19)$$

For  $|x-y| \ll \xi_c$ , Eq. (19) reduces to  $\exp(\beta^2|x-y|/\gamma)$ , so that for  $N \ll \xi_c$  we have

$$\langle \bar{t}_{0,N} \rangle \sim N^2 \exp(4\beta^2 \sigma^2 N/\xi_c). \quad (20)$$

(Here and in what follows, we measure distances in units of  $a$ , unless specified otherwise.) This kind of exponential creep is quite expected, since for  $\alpha \rightarrow 0$ ,  $\xi_c \rightarrow \infty$  our model (9a) and (9b) reduces to the random-force model.

In the opposite limit  $|x-y| \gg \xi_c$ , we can neglect the exponential  $e^{-|x-y|/\xi_c}$ , so that Eq. (18) produces an ordinary diffusion law, with a disorder-renormalized diffusion coefficient:

$$\langle \bar{t}_{0,N} \rangle = N^2 e^{4\beta^2 \sigma^2}. \quad (21)$$

Comparing Eqs. (21) and (15), we see that diffusion in a correlated potential profile proceeds more slowly than in an uncorrelated profile. It is straightforward to obtain an expression for the disorder-averaged MFPT for arbitrary correlation length. If we keep all four terms in the exponential in Eq. (14) while going to the continuum limit, we obtain

$$\bar{t}_{0,N} \approx 2 \int_0^N dx \int_x^N dy e^{\beta[U(x+a)+U(x)-U(y)-U(y-a)]}. \quad (22)$$

Averaging this expression over the disorder as in Eq. (19) yields for  $N \gg \xi_c$ :

$$\langle \bar{t}_{0,N} \rangle = N^2 \exp[2\beta^2 \sigma^2 (1 + e^{-a/\xi_c})], \quad (23)$$

which has the obvious limits of Eqs. (15) and (21) for  $\xi_c \rightarrow 0$  and  $\xi_c \gg a$ , respectively.

### III. TYPICAL VERSUS AVERAGE

Large deviations from the average are characteristic to many disordered systems. In this section, we therefore explore the *typical* properties of random walks as compared to the disorder-averaged ones.

#### A. Quantifying fluctuations

After the potential profile is generated (see Appendix B), we calculate the MFPT using Eq. (13). Figure 4(a) presents the mean first passage times calculated for various realizations of  $U(x)$  at biologically relevant temperature ( $\sigma \approx k_B T$ ). It is clear that although the ensemble-averaged MFPT does behave as prescribed by Eq. (23), typical MFPT exhibits high variability from one profile to another. The stepwise shape of typical curves suggests that a random walk in such a profile consists of regions characterized by subdiffusion (vertical “steps”) and superdiffusion (plateaus), appearing intermittently. Uncorrelated potential profiles, as Fig. 4(b) shows, also lead to a certain disorder-induced variability, though of a considerably smaller magnitude. To quantify the sample dependence of the MFPT, we calculate its variance over the ensemble of potential profiles. Figure 5 presents the standard deviation in  $\bar{t}_{0,N}$  as a function of  $N$  for correlated as well as uncorrelated potential profiles. We observe that the variance scales as  $N^3$  for all profiles. This dependence can be obtained analytically in a quite straightforward fashion. In a correlated profile, the MFPT is given by Eq. (18); then

$$\begin{aligned} \langle (\Delta \bar{t}_{0,N})^2 \rangle &\approx 4 \int_0^N dx \int_x^N dy \int_0^N dx' \\ &\times \int_{x'}^N dy' [ \langle e^{2\beta[U(x)-U(y)+U(x')-U(y')]} \rangle \\ &- \langle e^{2\beta[U(x)-U(y)]} \rangle \langle e^{2\beta[U(x')-U(y')]} \rangle ]. \end{aligned} \quad (24)$$

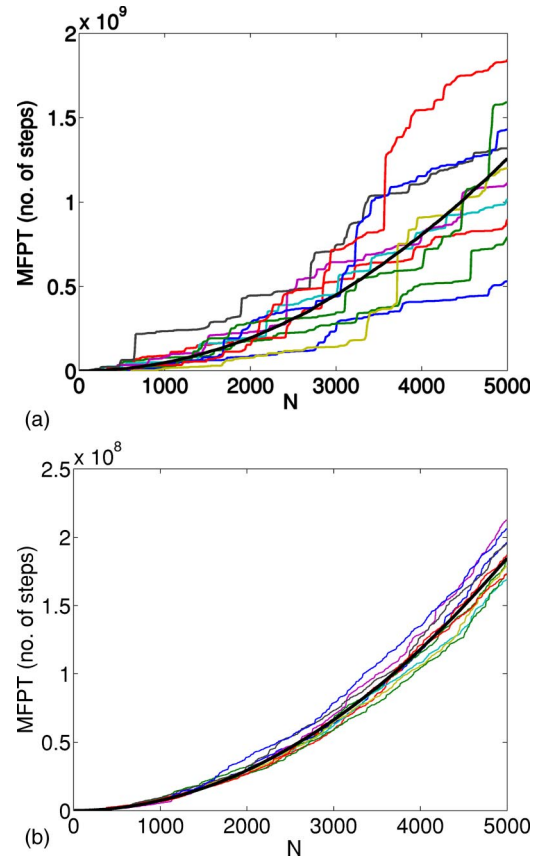


FIG. 4. (Color online) Mean first passage times: typical versus average. Thick solid lines are the result of averaging over 1000 realizations of potential profiles ( $\beta\sigma=1.0$ ): (a) correlated profile with  $\xi_c=40.0$ ; (b) uncorrelated profile.

We now recall that energies at points separated by distances larger than  $\xi_c$  are essentially independent. Therefore, to estimate the averages, we assume the energies to be equal for points within one correlation length and independent otherwise. The first average in the integral produces

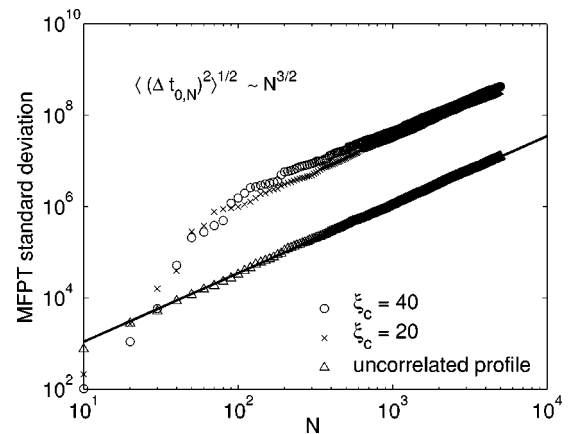


FIG. 5. MFPT standard deviation for  $\beta\sigma=1.0$  for correlated and uncorrelated potential profiles.

$$\begin{aligned}
 & \langle e^{2\beta[U(x)-U(y)+U(x')-U(y')]} \rangle \\
 & \simeq \langle e^{2\beta[U(x)-U(y)]} \rangle \langle e^{2\beta[U(x')-U(y')]} \rangle \\
 & \quad + \xi_c \delta(x-x') \langle e^{2\beta[2U(x)-U(y)]} \rangle \langle e^{-2\beta[U(y')]} \rangle \\
 & \quad + \xi_c \delta(y-y') \langle e^{-2\beta[2U(y)-U(x)]} \rangle \langle e^{2\beta[U(x')]} \rangle \\
 & \quad + \xi_c^2 \delta(x-x') \delta(y-y') \langle e^{-4\beta[U(y)-U(x)]} \rangle + \dots \\
 & \simeq \langle e^{2\beta[U(x)-U(y)]} \rangle \langle e^{2\beta[U(x')-U(y')]} \rangle + \xi_c e^{12\beta^2\sigma^2} [\delta(x-x') \\
 & \quad + \delta(y-y')] + \xi_c^2 e^{16\beta^2\sigma^2} \delta(x-x') \delta(y-y') + \dots. \quad (25)
 \end{aligned}$$

Plugging this expression into Eq. (24) and performing the integrations, we obtain the leading term

$$\langle (\Delta \bar{t}_{0,N})^2 \rangle \sim \xi_c N^3 e^{12\beta^2\sigma^2}. \quad (26)$$

Similar reasoning yields for the uncorrelated case

$$\langle (\Delta \bar{t}_{0,N})^2 \rangle \sim N^3 e^{6\beta^2\sigma^2}. \quad (27)$$

We see that for given  $\sigma$  and  $\beta$ , correlated energy landscapes produce stronger fluctuations in MFPT than uncorrelated ones, in agreement with Fig. 4.

Comparing the expressions for the variance with the corresponding expressions for disorder-averaged MFPT, we see that for any temperature, there is a characteristic distance  $N_c$ , below which there is no self-averaging and the typical MFPT is determined by fluctuations. This length is

$$N_c \sim \xi_c e^{4\beta^2\sigma^2} \quad (28)$$

for correlated profiles, and

$$N_c \sim e^{2\beta^2\sigma^2} \quad (29)$$

for uncorrelated ones. This effect is akin to “freezing” in the random-energy model [26]: for low enough temperatures, typical passage times for distances below  $N_c$  are dominated by high barriers. This is more pronounced for correlated profiles since in addition to stronger temperature dependence, there is amplification by a factor of  $\sim \xi_c$ , as sites within a correlation length give similar contributions. Figure 6 demonstrates the lack of self-averaging for uncorrelated potential profiles at short distances and low temperatures: the *median* MFPT (defined as the 50th percentile of a sample) shows large deviations from the average at distances shorter than  $N_c$  and coincides with it at distances larger than  $N_c$ .

### B. Anomalous diffusion

The lack of self-averaging in the region  $\xi_c \ll N \ll N_c$  can be quantified by estimating the typical MFPT. Consider Eq. (14) for an uncorrelated potential and define the following coarsening procedure:  $\tilde{U}_i = U_{2i} + U_{2i+1}$ . Then, in the “freezing regime,” the double sum

$$\sum_k \sum_i \exp[\beta(\tilde{U}_i - \tilde{U}_k)] \quad (30)$$

is dominated by  $(i, k)$  producing the largest exponent. For a finite sample  $\{U_j\}$  of size  $N$  and variance  $\sigma^2$ , the correspond-

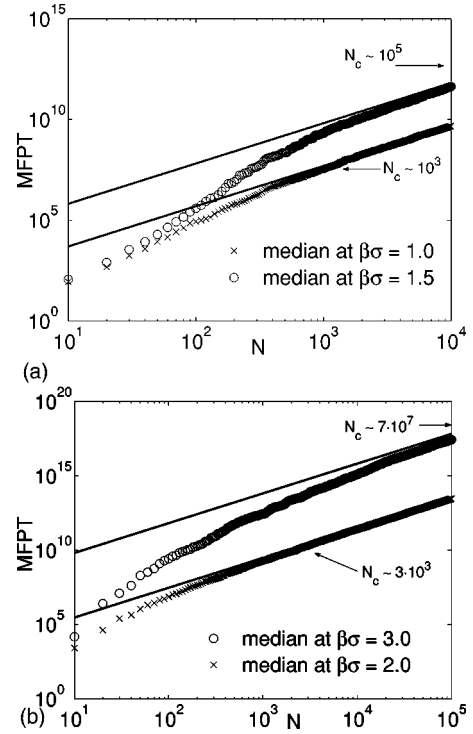


FIG. 6. Median versus disorder-averaged [solid lines calculated from Eq. (23)] MFPT. Median values were calculated for 1000 realizations of potential profiles: (a) Correlated potential profile with  $\xi_c = 20.0$ ; (b) uncorrelated potential profile.

ing sample  $\{\tilde{U}_i\}$  contains  $N/2$  values distributed with a variance  $2\sigma^2$ . The minimum and the maximum of  $\{\tilde{U}_i\}$  have therefore characteristic values of  $\pm 2\sigma \sqrt{\ln[N/(2\sqrt{2}\pi)]}$ , respectively. Thus, a typical MFPT for an uncorrelated potential reads

$$\bar{t}_{0,N} \sim \exp \left[ 4\beta\sigma \sqrt{\ln \frac{N}{2\sqrt{2}\pi}} \right]. \quad (31)$$

For the purposes of estimating the extreme values of a correlated energy landscape, the sample size is effectively reduced by a factor of  $\sim \xi_c$ , therefore, the extrema of  $\{U_i\}$  are approximately  $\pm \sigma \sqrt{2 \ln[N/(\xi_c \sqrt{2}\pi)]}$ . Noting that sites within a correlation length around the extrema contribute similarly to the MFPT, for a correlated potential we write

$$\bar{t}_{0,N} \sim \xi_c^2 \exp \left[ 4\beta\sigma \sqrt{2 \ln \frac{N}{\xi_c \sqrt{2}\pi}} \right]. \quad (32)$$

Figure 7 compares typical values of  $\bar{t}_{0,N}$  calculated from Eqs. (31) and (32) with numerically calculated median values of MFPT. We see that our analytical estimates produce a correct order of magnitude for  $\bar{t}_{0,N}$ . As expected, for uncorrelated profiles, the agreement is better at lower temperatures; for higher temperatures, Eq. (31) is an underestimation since we do not include contributions from second lowest, second highest, etc., energy levels. Eq. (32), on the other hand, turns out to be a slight overestimation, since we have replaced the

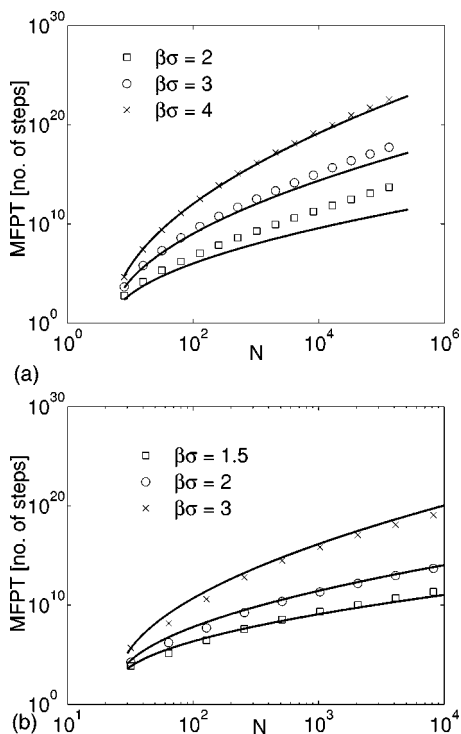


FIG. 7. Typical MFPT for  $N \leq N_c$  at various values of  $\beta\sigma$ : (a) Uncorrelated potential profile; (b) correlated potential profile with  $\xi_c = 10$ . Solid lines are the analytical estimates from Eqs. (31) and (32).

average of  $\sim \xi_c^2$  terms by their maximum value.

Large difference between the median and the average values is a signature of a broad (“fat tailed”) asymmetric probability distribution. The insets of Fig. 8 present two probability density functions for MFPT, at  $N \leq N_c$  and  $N \geq N_c$ . For short distances, the distribution is very broad and spans several orders of magnitude. For  $N \geq N_c$ , the system is self-averaging, in the sense that the MFPT distribution is much narrower with almost coinciding median and average values.

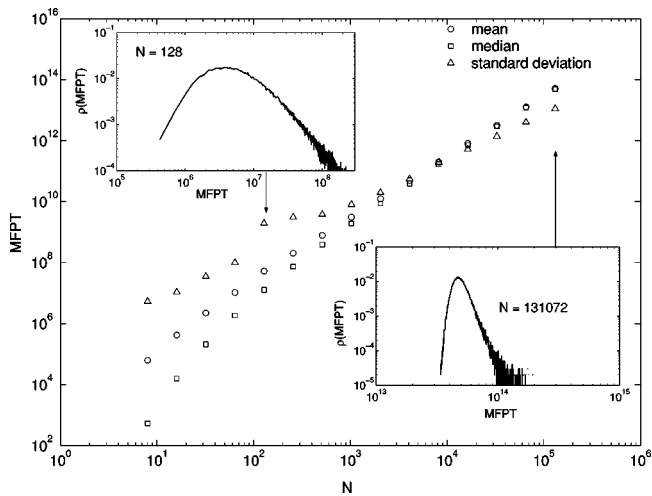


FIG. 8. Probability density functions for MFPT calculated for 100 000 uncorrelated profile realizations at  $\beta\sigma = 2$ .

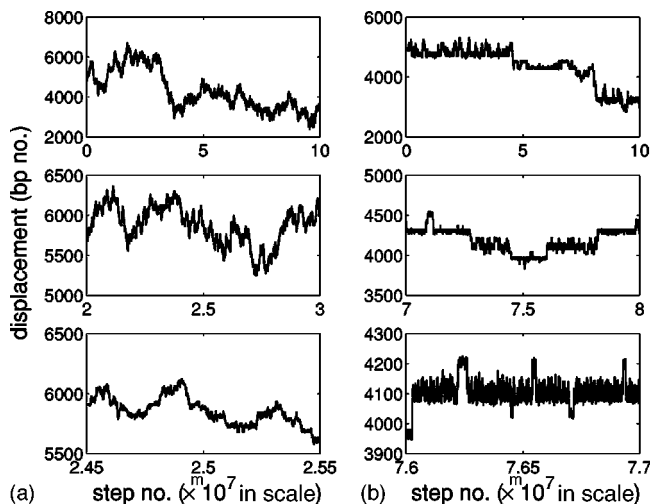


FIG. 9. Random walk in (a) uncorrelated, and (b) correlated with  $\xi_c = 20.0$ , potential energy profiles.

### C. Characteristics of random walk

To complete the picture, we perform direct simulations of random walks in correlated and uncorrelated potential profiles; typical results are depicted in Fig. 9. One can see a clear qualitative difference between the two cases: random walks in the uncorrelated profile look very much like standard walks with  $p_i = q_i = 1/2$ , whereas motion of a particle in a correlated profile has a somewhat different nature.

As above, we see that macroscopic motion of a particle in a correlated potential consists of subdiffusive as well as superdiffusive segments. It also appears that the particle tends to be localized near the bottom of “valleys” of few  $\xi_c$  in extent, whereas in an uncorrelated profile, there are no preferable sites for localization. Obviously, when the time is measured in real-time units, rather than in number of steps, the particle is more likely to be found at the minima of the energy landscape in both cases. In terms of the number of steps though, all sites of the uncorrelated landscape are revisited more or less uniformly.

## IV. BIOLOGICAL IMPLICATIONS

### A. Transcription factors

Consider a DNA-binding protein searching for its target site on the genome. As explained in the Introduction, a correlated random-energy landscape can arise from the interplay of sequence-dependent flexibility, and the bending contribution to the total DNA-binding energy. Diffusion on such a landscape may then lead to localization in the energy “valleys,” i.e., the protein will reside preferentially in specific (favorable) areas of the genome. Such nonuniform sampling has important implications for biological strategies of transcription factor bindings: First, if a valley contains several binding sites, the rapid (superdiffusive) scanning of the valley leads to quick equilibration between these sites (while equilibration for similarly spaced sites outside a valley will take much longer). This is important when the protein binds nearby sites with distinct binding energies, and the strongest

one has to be occupied first to provide correct regulation (as in the case of the *Cro* repressor). Second, several proteins bind their specific sites only when activated by ligands (e.g., *PurR*, *Gals*, etc.), spending the rest of the time in an inactive form “waiting” for the ligand. These proteins can benefit from staying close to the site in the waiting mode, since they can then quickly find their target upon activation.

One of the results of this study was that inhomogeneities significantly reduce the overall diffusion rate, as in Eq. (23). While this may be beneficial in confining a protein to favorable regions, it severely restricts the ability to search large portions of the genome by one dimensional diffusion. Since we argue that a portion of the inhomogeneity originates from variations in the bending energy of the DNA, a potential strategy is for the binding protein to switch between two states which bend the DNA weakly or strongly. The weak bending state is subject to reduced variations in the energy landscape and can diffuse more freely (search mode), compared to the strongly bending state which is more likely to be confined in the vicinity of favorable energy valleys (waiting mode). One potential candidate for exploiting this strategy is the tetrameric *LacI* protein that consists of two DNA-binding dimeric subunits. Each subunit binds DNA and bends it slightly; when both subunits are bound, DNA is deformed into an extended loop. Several experimental results suggest that *LacI* binds DNA with only one subunit while searching for its target site (“holding DNA with one arm”). Only when both subunits find their site, the DNA is bent into a loop. Very few structural data are available for proteins bind to DNA nonspecifically (search mode). The above strategy suggests that DNA is less deformed in such complexes.

Another potential source for a correlated inhomogeneous energy landscape is an extended protein–DNA interface with net interactions that are the sum of several local contributions. (The addition of such correlated contributions leads to a much larger variance of energy than if they were uncorrelated.) This can be a significant effect for large multiprotein complexes (such as polymerases, TFIID, TFIIB complexes in yeast, etc.). To avoid slow down by such inhomogeneities, protein complexes can avoid scanning DNA in the fully assembled state when the protein–DNA interface is extensive. Individual components of the complex can search for their sites independently, assembling the whole complex only on the right site. In fact, most of large protein–DNA complexes follow this strategy of assembly on the site, while many dimers and tetramers are assembled in the solution.

### B. Nucleosomes

Other implications concern nucleosome positioning and dynamics. Wrapping of the DNA around these large multiprotein complexes is essential for packing DNA in the small volume of the cell nucleus. Nucleosomes, however, prevent transcription factors and other proteins from accessing DNA. To allow a transcription factor to access its target, nucleosomes close to that site have to be removed from the DNA or repositioned. While removal of nucleosomes is made by specific enzymes that chemically modify them (e.g., by histone methylation), repositioning relies in part on nucleosome mo-

bility. In general, nucleosomes have to be (i) positioned at specified locations, and (ii) be able to move along the DNA in the vicinity to the initial placement site allowing access to this region of the DNA.

Nucleosome positioning is determined by specific sequences on the DNA. Such sequences are also known to provide DNA flexibility and/or internal curvature [23,36]. As discussed above, local DNA flexibility and curvature create a correlated energy landscape for binding. We suggest that inhomogeneous diffusion on such landscapes is an important element that provides both (i) preferential positioning of the nucleosomes due to DNA flexibility and curvature, and (ii) relatively rapid diffusion within the confines of the energy valley. Conversely, uncorrelated landscapes cannot achieve both objectives, since strong nucleosome binding sites prevent local diffusion along the DNA, while weak sites are not able to localize these proteins, leading to their random placement. In fact, experiments [36] have shown that nucleosome positioning sites are extended and are fairly weak. Such structure of positioning sites creates an extended valley on the correlated binding landscape, supporting our hypothesis.

This mechanism can also explain how certain proteins (such as HMGB) can reposition nucleosomes by binding to the DNA in their proximity. It has been suggested that such proteins alter the local mechanical properties of the DNA (such as its flexibility, curvature, or supercoiling) leading to repositioning of the nucleosome [37]. If the nucleosome is indeed preferentially localized by being trapped in a valley of the binding landscape, HMGB proteins may well alter the shape of the valley (e.g., by shrinking it on one side). Mobile nucleosomes, rapidly diffusing within the boundaries of the valley, will then reposition themselves in the new landscape.

### C. Translocation

In Sec. IB we described how slow (activated) passage of ssDNA through a nanopore can be modeled by diffusion over a correlated landscape. In particular, we demonstrated that if there are inhomogeneities in the charge of the DNA *inside the channel*, there will be variations in the potential energy landscape that are proportional to the applied voltage difference  $V$ . There is in fact scant structural information about the reconfigurations of charges (both free and bound) as DNA passes through a channel. Examining the variations in the MFPT of DNA as a function of the applied voltage [8], may provide an indirect probe of any inhomogeneities in the charge passing through a channel.

## V. CONCLUSIONS

We studied one-dimensional diffusion in a random-energy landscape with short-range correlations. We found that disorder with short correlation length  $\xi_c$  leads to a strong sample dependence of diffusion characteristics. The diffusive transport is influenced up to length scales exceeding  $\xi_c$  by orders of magnitude. Three diffusion regimes can be identified:

- (1) For distances smaller than the correlation length ( $N \ll \xi_c$ ), the disorder-averaged MFPT is

$$\langle \bar{t}_{0,N} \rangle \sim N^2 \exp(4\sigma^2 \beta^2 N / \xi_c).$$

At biologically relevant temperatures, the  $N^2$  factor prevails; however, at low temperatures ( $k_B T \lesssim 2\sigma / \sqrt{\xi_c}$ ), we obtain exponential creep (Sinai's diffusion).

(2) For distances  $N$  much larger than the characteristic value  $N_c$ , MFPT exhibits some variability from sample to sample. However, the typical value of the MFPT is given by the disorder-averaged MFPT:

$$\langle \bar{t}_{0,N} \rangle = N^2 \exp[2\beta^2 \sigma^2 (1 + e^{-a/\xi_c})].$$

The variance of MFPT over the ensemble of potential profile realizations scales as  $N^3$  with distance above  $N_c$ . The characteristic distance  $N_c$  equals  $\xi_c e^{4\beta^2 \sigma^2}$  for correlated profiles and  $e^{2\beta^2 \sigma^2}$  for uncorrelated ones.

(3) In the intermediate case  $\xi_c \ll N \ll N_c$ , the disorder-averaged MFPT behaves as described by Eq. (23). However, the MFPT distribution over the ensemble of profile realizations is much broader below  $N_c$  than above it, as Fig. 8 demonstrates. As a result, a typical sample yields diffusion times orders of magnitude shorter than the average. This effect can be qualitatively understood in terms of the random energy model. Below  $N_c$ , diffusion times are mostly influenced by high barriers and deep valleys that are at the extrema of energy landscape histogram. The typical diffusion times are given by

$$\bar{t}_{0,N} \sim \exp \left[ 4\beta\sigma \sqrt{\ln \frac{N}{2\sqrt{2\pi}}} \right]$$

for an uncorrelated profile, and

$$\bar{t}_{0,N} \sim \xi_c^2 \exp \left[ 4\beta\sigma \sqrt{2 \ln \frac{N}{\xi_c \sqrt{2\pi}}} \right],$$

for a correlated one. Above  $N_c$ , most obstacles to the particle motion lie in the central region, so that Eq. (23) produces a valid estimation for a typical diffusion time: the system becomes self-averaging.

These regimes appear to be relevant for biological systems and provide qualitative insight into the kinetics of protein-DNA interaction.

#### ACKNOWLEDGMENTS

This work was supported by the National Science Foundation through Grant No. DMR-01-18213 (M.K.). L.M. is also supported by a John F. and Virginia B. Taplin Award. M.S. is supported by NEC research fund.

#### APPENDIX A: MEAN FIRST-PASSAGE TIME DERIVATION

The MFPT from the 0th site to the  $N$ th site is defined as the mean number of steps the particle has to make in order to reach the  $N$ th site *for the first time*. The derivation here follows the one in Ref. [35].

Let  $P_{i,j}(n)$  denote the probability to start at the  $i$ th site and to reach the  $j$ th site for the first time in exactly  $n$  steps. Then,

for example, any path contributing to  $P_{i,i+1}(n)$  should end with a step from the  $i$ th site to the right, i.e.,

$$P_{i,i+1}(n) = p_i T_i(n-1), \quad (\text{A1})$$

where  $T_i(n)$  is defined as the probability of returning to the  $i$ th site after  $n$  steps *without stepping to the right of it*. Now, all the paths contributing to  $T_i(n-1)$  should *start* with a step to the left, i.e., to the  $(i-1)$ th site with probability  $q_i$ , and then returning to the  $i$ th site in the remaining  $n-2$  steps, *not necessarily for the first time*. Any path possessing these properties consists of paths that originate from the  $(i-1)$ th site and reach the  $i$ th site for the first time in  $m \leq (n-2)$  steps and paths that originate from the  $i$ th site and return to the  $i$ th site in  $(n-m-2)$  steps without stepping to the right of it. Thus, the probability  $T_i(n-1)$  can be written as

$$T_i(n-1) = q_i \sum_{m,l} P_{i-1,i}(m) T_i(l) \delta_{m+l,n-2}. \quad (\text{A2})$$

We now introduce generating functions

$$\tilde{P}_{i,j}(z) = \sum_{n=0}^{\infty} z^n P_{i,j}(n), \quad \tilde{T}_i(z) = \sum_{n=0}^{\infty} z^n T_i(n). \quad (\text{A3})$$

One can easily show (see, e.g., Ref. [38]) that

$$\tilde{P}_{0,N}(z) = \prod_{i=0}^{N-1} \tilde{P}_{i,i+1}(z). \quad (\text{A4})$$

Knowing  $\tilde{P}_{i,i+1}(z)$ , one calculates the MFPT straightforwardly as

$$\begin{aligned} \bar{t}_{0,N} &= \frac{\sum_n n P_{0,N}(n)}{\sum_n P_{0,N}(n)} = \left[ \frac{d}{dz} \ln \tilde{P}_{0,N}(z) \right]_{z=1} \\ &= \sum_{i=0}^{N-1} \left[ \frac{d}{dz} \ln \tilde{P}_{i,i+1}(z) \right]_{z=1}. \end{aligned} \quad (\text{A5})$$

Using Eqs. (A1) and (A2), we obtain the following recursion relation for  $\tilde{P}_{i,i+1}(z)$ :

$$\tilde{P}_{i,i+1}(z) = \frac{z p_i}{1 - z q_i \tilde{P}_{i-1,i}(z)}. \quad (\text{A6})$$

To solve for  $\bar{t}_{0,N}$ , we must introduce boundary conditions. Let  $p_0=1, q_0=0$ , which is equivalent to introducing a reflecting wall at  $i=0$ . This boundary condition clearly influences the solution for short times and distances. However, as numerical simulations suggest, its influence relaxes quite fast, so that for longer times, the result is clearly independent of the boundary. The benefit of setting  $p_0=1$  becomes clear when we observe that

$$\tilde{P}_{0,1}(1) = 1, \quad \Rightarrow \quad \forall i \quad \tilde{P}_{i,i+1}(1) = 1. \quad (\text{A7})$$

Hence,

$$\bar{t}_{0,N} = \sum_{i=0}^{N-1} \tilde{P}_{i,i+1}(1). \quad (\text{A8})$$

The recursion relation for  $P_{i,i+1}(1)$  is readily obtained from Eq. (A6):

$$\tilde{P}'_{i,i+1}(1) = \frac{1}{p_i} + \frac{q_i}{p_i} \tilde{P}'_{i-1,i}(1) = 1 + \omega_i [1 + \tilde{P}'_{i-1,i}(1)] \quad (\text{A9})$$

with  $\omega_i \equiv q_i/p_i$ . Thus, the expression for  $\bar{t}_{0,N}$  is obtained in the closed form as

$$\bar{t}_{0,N} = N + \sum_{k=0}^{N-1} \omega_k + \sum_{k=0}^{N-2} \sum_{i=k+1}^{N-1} (1 + \omega_k) \prod_{j=k+1}^i \omega_j. \quad (\text{A10})$$

## APPENDIX B: POTENTIAL PROFILE GENERATION

Given the pseudoenergy partition function

$$Z(\lambda) = \int \mathcal{D}[U] e^{-\lambda \mathcal{H}[U]}, \quad (\text{B1})$$

the average pseudoenergy is

$$\langle \mathcal{H} \rangle = - \left. \frac{\partial}{\partial \lambda} \ln Z(\lambda) \right|_{\lambda=1}, \quad (\text{B2})$$

and the variance is

$$\langle (\Delta \mathcal{H})^2 \rangle = \langle \mathcal{H}^2 \rangle - \langle \mathcal{H} \rangle^2 = \left. \frac{\partial^2}{\partial \lambda^2} \ln Z(\lambda) \right|_{\lambda=1}. \quad (\text{B3})$$

Straightforward calculation for the pseudoenergy given by Eqs. (9a) and (9b) yields

$$Z(\lambda) = \prod_q \frac{1}{\sqrt{2\pi\lambda(\alpha + \gamma q^2)}}. \quad (\text{B4})$$

Since a discrete chain of length  $L$  has exactly  $L$  modes, each contributing a factor of  $\lambda^{-1/2}$ , we have

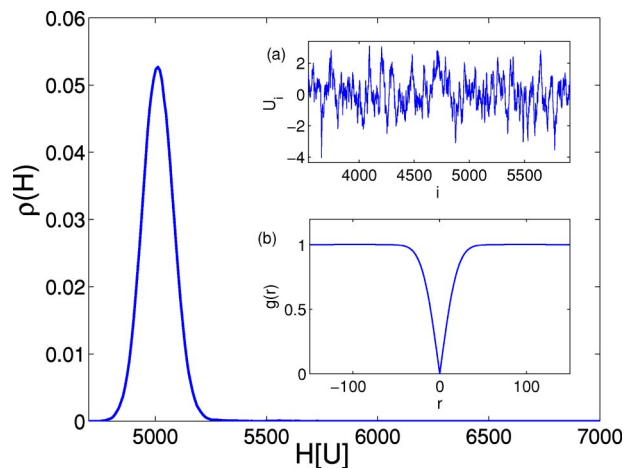


FIG. 10. Pseudoenergy probability density for a profile of length  $L=10\,000$ , with  $\sigma=1.0$ ,  $\xi_c=20.0$ . Insets: (a) Typical potential profile; (b) potential profile correlator  $g(r)=1/2[U(x)-U(x+r)]^2$ ; the averaging was performed over 1000 profile realizations.

$$\ln Z(\lambda) = -\frac{L}{2} \ln \lambda + A, \quad (\text{B5})$$

where  $A$  does not depend on  $\lambda$ . Thus,

$$\langle \mathcal{H} \rangle = L/2, \quad \langle (\Delta \mathcal{H})^2 \rangle = L/2. \quad (\text{B6})$$

Hence, typical potential profiles have pseudoenergies in the range  $L/2 \pm \sqrt{L/2}$ . This result together with Gaussian statistics of energy levels of Eq. (10) forms the basis of the algorithm we employ for building the energy profiles. First, a random and uncorrelated potential profile obeying Gaussian statistics with the required variance  $\sigma^2$  is generated on a one-dimensional lattice. Next, we look for a permutation of lattice sites that produces a typical pseudoenergy  $\mathcal{H}[U]$  for a given correlation length  $\xi_c$  (or, equivalently, for given values of  $\alpha$  and  $\gamma$ ). This is accomplished by a Metropolis-type algorithm that converges to a prescribed value of pseudoenergy picked at random from Gaussian distribution around  $\langle \mathcal{H} \rangle$ ; see Fig. 10.

- 
- [1] J. D. Murray, *Mathematical Biology* (Springer-Verlag, Berlin, 2002).
- [2] C. Bustamante, D. Keller, and G. Oster, *Acc. Chem. Res.* **34**, 412 (2001).
- [3] R. D. Vale and R. A. Milligan, *Science* **288**, 88 (2000).
- [4] R. D. Astumian, *Science* **276**, 917 (1997).
- [5] D. K. Lubensky and D. R. Nelson, *Biophys. J.* **77**, 1824 (1999).
- [6] P. G. de Gennes, *Physica A* **274**, 1 (1999).
- [7] H. Salman, D. Zbaida, Y. Rabin, D. Chatenay, and M. Elbaum, *Proc. Natl. Acad. Sci. U.S.A.* **98**, 7247 (2001).
- [8] A. Meller, L. Nivon, and D. Branton, *Phys. Rev. Lett.* **86**, 3435 (2001).
- [9] O. G. Berg, R. B. Winter, and P. H. von Hippel, *Biochemistry* **20**, 6929 (1981).
- [10] P. H. von Hippel and O. G. Berg, *J. Biol. Chem.* **264**, 675 (1989).
- [11] N. Shimamoto, *J. Biol. Chem.* **274**, 15293 (1999).
- [12] O. G. Berg and P. H. von Hippel, *J. Mol. Biol.* **193**, 723 (1987).
- [13] U. Gerland, J. D. Moroz, and T. Hwa, *Proc. Natl. Acad. Sci. U.S.A.* **99**, 12 015 (2002).
- [14] R. F. Bruinsma, *Physica A* **313**, 211 (2002).
- [15] D. A. Erie, G. Yang, H. C. Schultz, and C. Bustamante, *Science* **266**, 1562 (1994).
- [16] M. G. Munteanu, K. Vlahoviček, S. Parthasarathya, I. Simon, and S. Pongor, *Trends Biochem. Sci.* **23**, 341 (1998).
- [17] K. Vlahoviček, L. Kaján, and S. Pongor, *Nucleic Acids Res.* **13**, 3686 (2003), <http://www.icgeb.trieste.it/dna/>
- [18] I. Brukner, R. Sanchez, D. Suck, and S. Pongor, *EMBO J.* **14**,

- 1812 (1995).
- [19] A. Gabrielian and S. Pongor, FEBS Lett. **393**, 65 (1996).
- [20] H. Schiessel, J. Widom, R. F. Bruinsma, and W. M. Gelbart, Phys. Rev. Lett. **86**, 4414 (2001).
- [21] J. Widom, Annu. Rev. Biophys. Biomol. Struct. **27**, 285 (1998).
- [22] J. Widom, Q. Rev. Biophys. **34**, 269 (2001).
- [23] R. Kiyama and E. N. Trifonov, FEBS Lett. **523**, 7 (2002).
- [24] D. Cule and T. Hwa, Phys. Rev. Lett. **80**, 3145 (1998).
- [25] A. Meller, J. Phys.: Condens. Matter **15**, R581 (2003).
- [26] B. Derrida, Phys. Rev. B **24**, 2613 (1981).
- [27] J. Bryngelson and P. Wolynes, Proc. Natl. Acad. Sci. U.S.A. **84**, 7524 (1987).
- [28] J. P. Bouchaud, A. Comtet, A. Georges, and P. Le Doussal, Ann. Phys. (N.Y.) **201**, 285 (1990).
- [29] P. G. De Gennes, J. Stat. Phys. **12**, 463 (1975).
- [30] P. Le Doussal and V. M. Vinokur, Physica C **254**, 63 (1995).
- [31] D. S. Fisher, P. Le Doussal, and C. Monthus, Phys. Rev. Lett. **80**, 3539 (1998).
- [32] T. Hwa, E. Marinari, K. Sneppen, and L. Tang, Proc. Natl. Acad. Sci. U.S.A. **100**, 4411 (2003).
- [33] Y. G. Sinai, Theor. Probab. Appl. **27**, 247 (1982).
- [34] S. H. Noskowitz and I. Goldhirsh, Phys. Rev. Lett. **61**, 500 (1988).
- [35] K. P. N. Murthy and K. W. Kehr, Phys. Rev. A **40**, 2082 (1989); **41**, 1160 (1990).
- [36] A. Thastrom, P. T. Lowary, H. R. Widlund, H. Cao, M. Kubista, and J. Widom, J. Mol. Biol. **288**, 213 (1999).
- [37] A. A. Travers, EMBO Rep. **4**, 131 (2003).
- [38] I. Goldhirsh and Y. Gefen, Phys. Rev. A **33**, 2583 (1986).
- [39] DNA bending by transcription factors is a well-known phenomenon, though practically all the available experimental data focus on proteins bound to operator sequences.
- [40] For  $\alpha$  haemolysin, the diameter of the limiting aperture is about 15 Å.